ROYAL SOCIETY OF CHEMISTRY

EDGE ARTICLE

Check for updates

All publication charges for this article have been paid for by the Royal Society of Chemistry

Manipulating dynamic covalent bonds through direct photoisomerization

Neil D. Dolinski, [†*a] Alex E. Crolais,[†b] Nicholas R. Boynton,[a] Chuqiao Chen, [a] Juan J. de Pablo,[acde] Scott A. Snyder [*b] and Stuart J. Rowan [*ab]

The wide availability, ease of manipulation, and access to spatiotemporal control make light an attractive stimulus for controlling dynamic covalent chemistries/networks. In this work, a series of photo-isomerizable benzalisoxazolone (BIOx) thia-Michael (tM) acceptors were developed that exhibit an increase in thiol-bonding during irradiation with visible light (455–470 nm). *In situ* photo-NMR experiments demonstrate significant increases in the overall system K_{eq} (extent of bonding) for a variety of electronically-substituted BIOx tM acceptors. A combination of experimental and computational studies show that steric interactions between the β-phenyl ring and substituent on the isoxazolone in the *E*-isomer serve as a driving force for the increased K_{eq}. In addition, it is demonstrated that the power/intensity of the light can be used to tune the system's response. Incorporation of these photoisomerizable motifs into dynamic polymer networks gives access to organogels that exhibit reversible, on-demand, light-triggered stiffening.

Introduction

By virtue of their reversible and stimulus-responsive nature,[1] dynamic covalent chemistries (DCCs) have seen widespread use in applications ranging from drug delivery systems,[2,3] adhesives,[4,5] (re)processability/recyclability,[6,7] and smart/adaptive materials.[8] The wide suite of currently available DCCs include reversible Diels–Alder reactions,[9–11] disulfide/diselenide exchange,[12,13] and transesterifications,[14,15] to name just a few.[16–19] Available DCCs cover a wide range of bonding partners with varying characteristics such as exchange mechanism, equilibrium constants, exchange rate(s), catalyst requirements, and the nature of the external stimulus (*e.g.*, heat, pH, light, *etc.*) required to induce a response.[20,21] The choice of which dynamic covalent bond to incorporate into a polymeric system is critical, as this will determine key properties of the material.

Light has several attractive features over other stimuli, including the ability to modulate wavelength and intensity, and access to spatiotemporal control. Photoswitches (PSs), a privileged class of compounds that undergo (bi)directional switching in response to light, can undergo a variety of

transformations ranging from changes in molecular shape (*e.g.*, *E*/*Z* photoisomerization), conjugation, charge, or even pK_a.[22] Recent studies have elegantly demonstrated that coupling PS groups (*e.g.*, azobenzenes,[23–25] hydrazones,[26,27] spiropyrans,[28] and diarylethenes[29,30]) in close proximity to a dynamic covalent bond allows for manipulation of bond exchange. Often the PS moiety is not directly involved in the dynamic bonding itself, but modulates the dynamic bond through secondary interactions. An elegant example of this is a photoswitchable azobenzene–boronic ester system developed by the Kalow group that leverages the photoisomerization of azobenzene (from *trans* to *cis*) to result in an increase in diol bonding due to destabilization of the unbonded *cis* boronic acid and stabilization of the bonded ester relative to the *trans* isomer (Fig. 1A).[24] Given the utility of such systems it is of interest to explore the development of synthetically-simple, tunable, light-responsive dynamic bonds.

In recent years, thia-Michael (tM) chemistry, the conjugate addition of a thiol to an activated alkene, has seen exciting applications beyond its traditional use of forming a static C–S bond.[31] Through tailoring the substituents on the activated alkene, the dynamic behavior of the tM bond can be readily tuned, leading to a range of reported dynamic tM polymer networks.[32–34] In many of these systems, elevated temperatures and/or the presence of base are required to access dynamic exchange. There is an interesting subset of tM acceptors, such as benzalcyanoacetate (BCA),[35] benzalcyanoacetamide (BCAm),[36] and benzalisoxazolone (BIOx),[37] which can undergo catalyst-free, room-temperature thiol exchange. The exploration of these systems has helped spearhead investigations into the

ªPritzker School of Molecular Engineering, University of Chicago, Chicago, Illinois 60637, USA. E-mail: stuartrowan@uchicago.edu; n.dolinski@columbia.edu

ᵇDepartment of Chemistry, University of Chicago, Chicago, Illinois 60637, USA. E-mail: sasnyder@uchicago.edu

ᶜDepartment of Chemical and Biomolecular Engineering, New York University, Brooklyn, NY 11201, USA

ᵈDepartment of Computer Science, New York University, NY 10012, USA

ᵉDepartment of Physics, New York University, NY 10012, USA
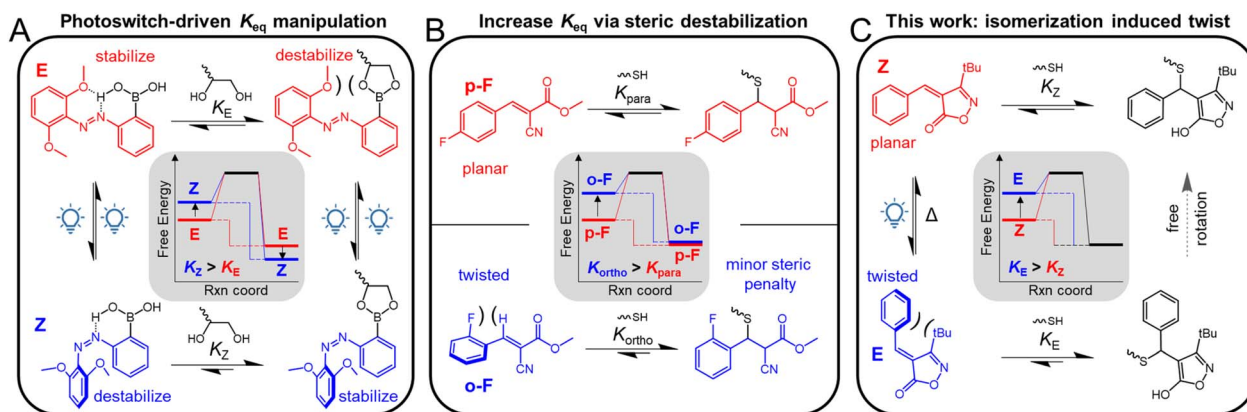
† These authors contributed equally.

Fig. 1 (A) Photoswitchable azobenzene boronic acid/ester system demonstrating the separation of the photoswitch and the dynamic covalent bond. (B) Increased thiol-bonding of *ortho*-substituted BCA acceptors compared to *para*-substituted BCA acceptors on account of destabilization of the free acceptor. (C) Proposed photoswitchable isoxazolone system with a destabilized free acceptor upon photoisomerization.

use of room temperature dynamic bonds in materials with applications including hydrogels,[38–40] colloidal systems,[41–43] and pluripotent materials.[44] Importantly, the equilibrium constant (K_{eq}) of these acceptors, and thus the thermomechanical properties of their derived materials, can modularly be tuned through electronic modifications of their β-phenyl rings.[45] Recently, it has been demonstrated that *ortho* substitution of the β-phenyl ring can be leveraged to significantly enhance the K_{eq} of these tM acceptors.[46] Careful selection of *ortho* substituents allows for the destabilization of the otherwise planar tM acceptor through twisting of the β-phenyl ring, while only minorly destabilizing the thiol-adduct. This results in an overall net increase in ΔG, and therefore K_{eq} (Fig. 1B).

Reported herein is an investigation that builds on these prior studies by exploring if photoisomerization of a sterically twisted isomer would allow light to be used to increase the K_{eq} of a dynamic tM system on demand. Specifically, the study focuses on how the *Z*-to-*E* photoisomerization of sterically hindered BIOx acceptors can be used to modulate the equilibrium of dynamic tM reactions (Fig. 1C). The synthesis of such BIOx acceptors is both facile and modular, which allows access to derivatives with a range of electronic and steric modifications. Importantly, this demonstration of sterics-focused molecular design has the potential to introduce photo-responsive behaviors across other DCC motifs, simplifying synthesis and offering new design handles for researchers.

Results and discussion

Synthesis of the targeted acceptors can be accomplished in two steps from readily available starting materials: (i) a ring closure between the appropriate alkyl (–X) keto ester and hydroxylamine followed by (ii) a Knoevenagel condensation with the appropriate substituted (–R) benzaldehyde (Fig. 2A) (see the SI for full synthetic details). Throughout this work, the prepared acceptors are denoted as **1R$_X$**, where R represents the substituent on the β-phenyl ring and X is the bulky alkyl group at the 3-position of the isoxazolone. A signature feature of the BCA, BCAm, or

BIOx-based tM acceptors is their ability to tune equilibrium and exchange kinetics through the addition of electronic substituents to the β-phenyl ring.[45] To explore if this important characteristic is maintained, a series of **1R$_{tBu}$** acceptors were prepared with a range of electronic substituents (–OMe, –Me, –H, and –Cl) at the –R position. Gratifyingly, in agreement with previous findings, the measured (dark) equilibrium constants ($K_{eq,Z}$) were found to have a linear relationship with σ^+ Hammett parameters,[37,45] with $K_{eq,Z}$ values ranging from 85 to 2950 M^{-1} for **1OMe$_{tBu}$** and **1Cl$_{tBu}$**, respectively (Fig. 2C). Furthermore, the determined slope (ρ) of 1.65 is intermediate between those of previously reported BIOx (2.08 (ref. 37)) and BCA (1.37 (ref. 45)) systems.

To determine ideal wavelengths to irradiate the suite of **1R$_X$** acceptors, UV-vis studies were carried out over a range of concentrations in DMSO (Fig. S1–S3). It was determined that blue light, either 455 or 470 nm depending on the –R
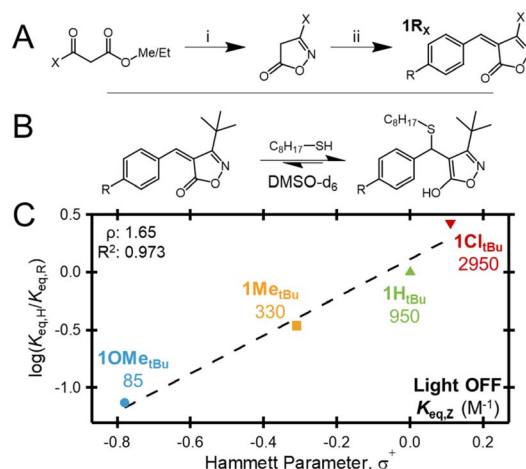

Fig. 2 (A) Synthesis of **1R$_x$** acceptors: (i) ketoester, hydroxylamine hydrochloride, NaOAc, ethanol, 50 °C; (ii) isoxazolone, benzaldehyde, piperidine, isopropanol, 50 °C. (B) Equilibrium between **1R$_{tBu}$** acceptors and **OT**. (C) Hammett plot of *Z* isomers of **1R$_{tBu}$** acceptors *versus* the σ^+ Hammett parameter of R.

modification (only R = OMe requiring 470 nm), would be most suitable for further study. Indeed, upon exposure to these wavelengths, new *E*-isomer peaks were readily observed *via* NMR and were found to rapidly disappear when the light was turned off (Fig. S4).

As an initial investigation into the impact of photo-isomerization on the reaction equilibrium, a 100 mM equimolar mixture of **1H$_{tBu}$** and 1-octanethiol (**OT**) was prepared and allowed to equilibrate in the dark for 12 hours prior to evaluation. During irradiation, the planar, energetically favorable *Z*-isomer undergoes isomerization to the twisted higher energy *E*-isomer.

This destabilization of the unbonded state should, in turn, shift the equilibrium of the reaction to the bonded state (Fig. 3A). Importantly, the bonded state is free to rotate, and should rapidly revert to its lowest energy configuration (in line

with the *Z* isomer), allowing the system to return to the initial equilibrium ($K_{eq,Z}$) after the light is turned off. To monitor this process in real time, a previously reported fiber-coupled NMR technique was adopted, as schematically shown in Fig. 3B.[47]

In agreement with expectations, the NMR spectrum of the equilibrated **1H$_{tBu}$** sample (dark) was found to have only peaks related to the unbound *Z* isomer (H$_{A,Z}$ @ 8.23 ppm and H$_{B,Z}$ @ 8.32 ppm) and the corresponding thiol adduct (H$_C$ @ 5.10 ppm), Fig. 3C. However, upon irradiating the sample with 455 nm light (14 mW), rapid *Z* to *E* isomerization was observed, yielding a new characteristic peak at 8.21 ppm (H$_{A,E}$) and an *E* isomer mole fraction of *ca.* 0.3. At this early stage of irradiation, a small increase in the fraction of thiol adducts was measured, described most conveniently by the overall system equilibrium constant, $K_{eq,sys}$ (not distinguishing between isomers), as defined below.

$$K_{eq,sys} = \frac{[\text{adduct}]}{[\text{unbound } \mathbf{1R_X}][\mathbf{OT}]} = \frac{[\text{adduct}]}{[\text{unbound } \mathbf{1R_X}]^2}$$

For the **1R$_{tBu}$** system $K_{eq,sys} = K_{eq,Z}$ in the dark as **1R$_{tBu}$** exists as the 100% *Z* isomer. Irradiation with light results in the appearance of a peak in the NMR consistent with the formation of the *E* isomer, along with a slight increase in $K_{eq,sys}$. An additional 20 minutes of irradiation was found to significantly increase $K_{eq,sys}$ from its initial (dark) value of 950 to 3300 M^{-1}, all while maintaining a consistent mole fraction of the *E* isomer. At this point, irradiation was ceased and the sample was allowed to equilibrate for 40 minutes. As expected, without irradiation, *E* isomer peaks vanished and the system returned to its initial dark equilibrium position.

To further investigate the performance of this system, the experiment was repeated under cycling conditions with continuous monitoring under the same irradiation conditions (455 nm, 14 mW), Fig. 3D. As before, upon irradiation the fraction of *E* isomer rapidly increased to *ca.* 30%, while the $K_{eq,sys}$ was found to gradually increase with exposure time. Upon turning the light off, *E* isomer peaks rapidly vanished and the $K_{eq,sys}$ returned back to the initial value. Importantly, these features were found to be consistent across cycles, implying that this strategy for manipulating dynamic bonds is reversible.

With the ability to control bonding through light demonstrated using **1H$_{tBu}$**, attention was next turned to other electronically-modified derivatives, **1R$_{tBu}$** (Fig. 4A). As the dark $K_{eq,Z}$ for the different derivatives spans a wide range, a fixed concentration of 40 mM was chosen to optimize the NMR signal and penetration depth across species. Importantly, all **1R$_{tBu}$** derivatives were found to experience significant shifts in bonding upon irradiation with the appropriate wavelength. Notably, for all but **1OMe$_{tBu}$**, irradiation to a consistent mole fraction of 0.30–0.35 *E* isomers drives a 3-fold increase in $K_{eq,sys}$ from the initial $K_{eq,Z}$, returning to the initial equilibrium state after irradiation is ceased. In the case of **1OMe$_{tBu}$**, an impressive 5× shift in $K_{eq,sys}$ was measured, despite a much smaller fraction of *E* isomer (*ca.* 0.15). This lower extent of isomerization is partially attributed to limited penetration depth on account of
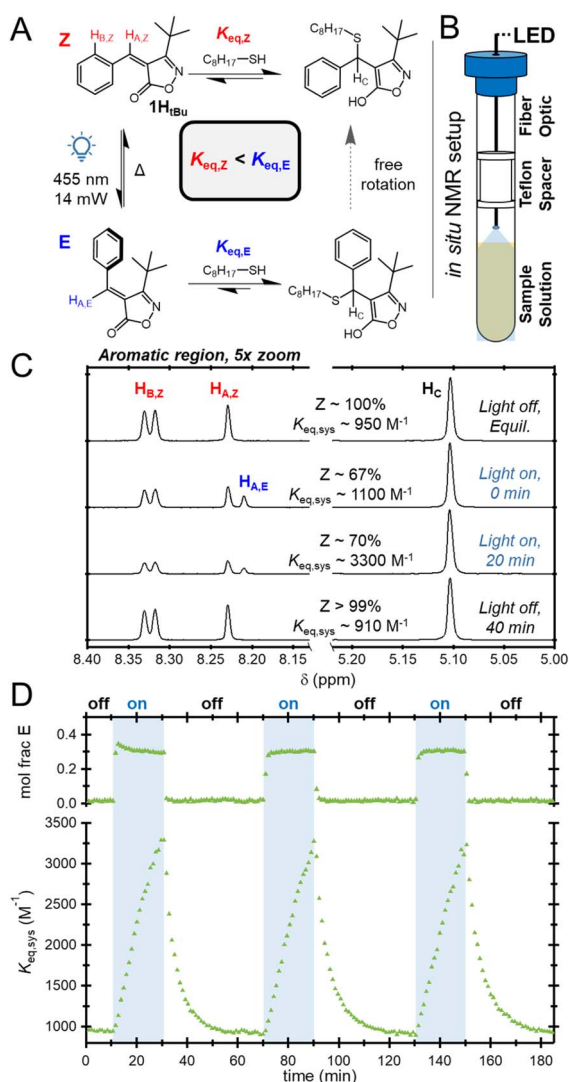

Fig. 3 (A) Equilibria involved in thiol-bonding and photoisomerization. (B) Diagram of the *in situ* LED NMR setup. (C) ^{1}H NMR spectra of **1H$_{tBu}$** equilibrated with **OT** without and during irradiation with 455 nm light. (D) Cycling experiment (455 nm irradiation for 20 min followed by a 40 min dark interval) for **1H$_{tBu}$** equilibrated with **OT**.
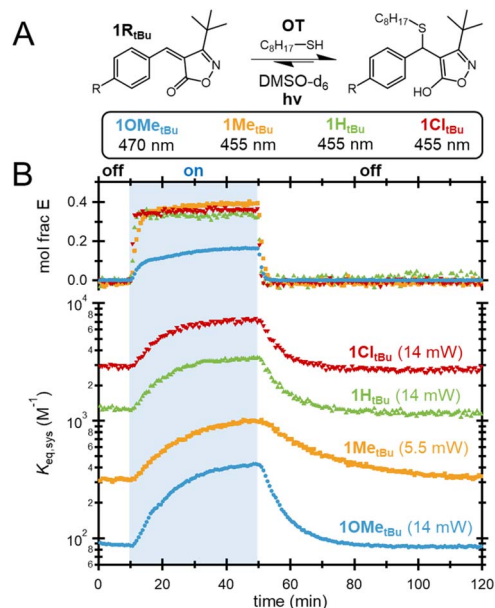
Fig. 4 (A) Equilibrium between **1R$_{tBu}$** and **OT**. (B) Mole fraction of the Z isomer and overall system K_{eq} ($K_{eq,sys}$) of **1R$_{tBu}$** acceptors equilibrated with **OT** during the NMR photoisomerization experiment.

the low $K_{eq,Z}$ yielding a higher concentration of absorbing unbound species.

Notably, during the previous suite of measurements, it was found that significantly less LED power was required to drive **1Me$_{tBu}$** to a similar mole fraction of E isomer as the other species sensitive to 455 nm light (5.5 vs. 14 mW). As such, a series of experiments with varied LED output power was carried out on **1OMe$_{tBu}$** (Fig. 5A and B) and **1Me$_{tBu}$** (Fig. S9). Intuitively, increased LED power was found to increase the E isomer population, in turn driving larger increases in $K_{eq,sys}$. Pleasingly, for both species, the isomer fraction and the maximum $K_{eq,sys}$ were found to be effectively linear with respect to LED power under the measured conditions, Fig. 5C. This feature is beneficial as it can serve as an additional tuning handle for the predictable manipulation of bonding.

To develop a better understanding of the underlying thermodynamic driving force, a series of acceptors with varied steric demand **1OMe$_X$** (–X = –Me, –iPr, and –tBu) were investigated via a combination of experiments and simulations. Equilibrated mixtures of **1OMe$_X$** and **OT** were investigated under fixed 14 mW irradiation conditions (Fig. 6A). The less hindered **1OMe$_{iPr}$** was found to undergo comparable Z to E isomerization to **1OMe$_{tBu}$** during exposure; however the overall $K_{eq,sys}$ was only minorly impacted, rising from ca. 90 to 150 M^{-1} (Fig. 6B). The least hindered species, **1OMe$_{Me}$**, did not undergo any measurable photoisomerization during irradiation, and was found to exhibit ca. 2 mole percent of E isomer throughout the experiment (Fig. S10).

To further explore the impact of the X-substituent on the photoisomerization, computational studies on the suite of **1OMe$_X$** acceptors were carried out. Density functional theory (DFT) calculations were performed using the Gaussian 16
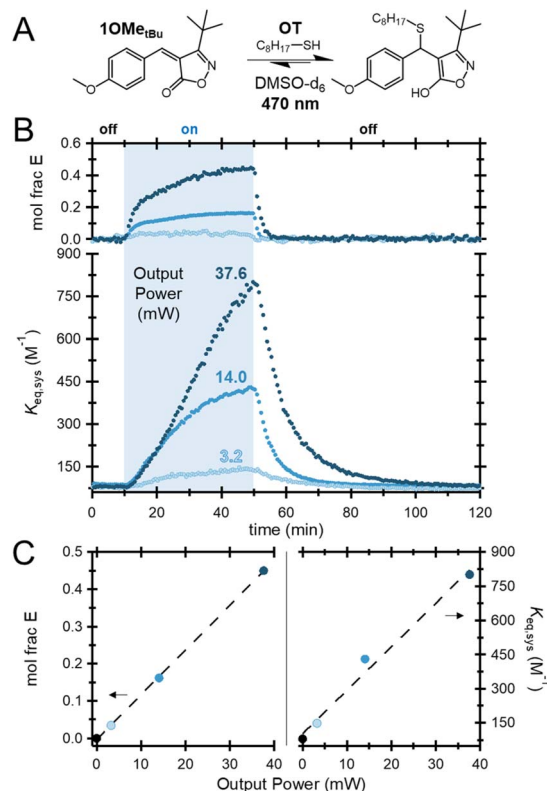

Fig. 5 (A) Equilibrium between **1OMe$_{tBu}$** and **OT**. (B) Mole fraction of the Z isomer and overall system K_{eq} ($K_{eq,sys}$) of **1OMe$_{tBu}$** equilibrated with **OT** during the NMR photoisomerization experiment at varying LED output powers (3.2 to 37.6 mW). (C) Mole fraction of Z isomer and maximum system K_{eq} versus LED output power.

package with the M06-2X/6-311+G(d,p) level of theory.[48] The free energy differences were computed in a vacuum and in DMSO with continuum solvent models (see the SI for details).[49] Representative configurations of Z and E isomers for the tBu acceptor as well as the thiol adduct are shown in Fig. 6C (the related configurations for **1OMe$_{Me}$** and **1OMe$_{iPr}$** are shown in Fig. S11). For all Z isomers, the dihedral angle between the phenyl group and the isoxazolone ring is close to 0 across the series suggesting that added steric bulk at the X position does not impact the stable Z-isomer. In contrast, the dihedral angle for the E-isomers across the series was found to significantly increase with the size of the alkyl substituent (Fig. 6D). Both simulations and calculations from experimental data found that all E-isomers possess higher free energy than the corresponding Z-isomers, attributed to steric repulsion between the alkyl (–X) group and the phenyl ring. This difference in free energy between Z- and E-isomers ($\Delta\Delta G_{Z,E}$) was found to increase from 9.6 to 26 kJ per mol (experimental) or from 8.4 to 19.2 kJ per mol (DFT) as the –X group increased in steric bulk from –Me to –tBu (Fig. 6E). In agreement with the initial hypothesis, increased steric demand (quantified through steric A-values, the ΔG value between different conformations of a substituted cyclohexane) results in a linear increase in $\Delta\Delta G_{Z,E}$, in turn leading to larger changes in $K_{eq,sys}$ (Fig. 6F).
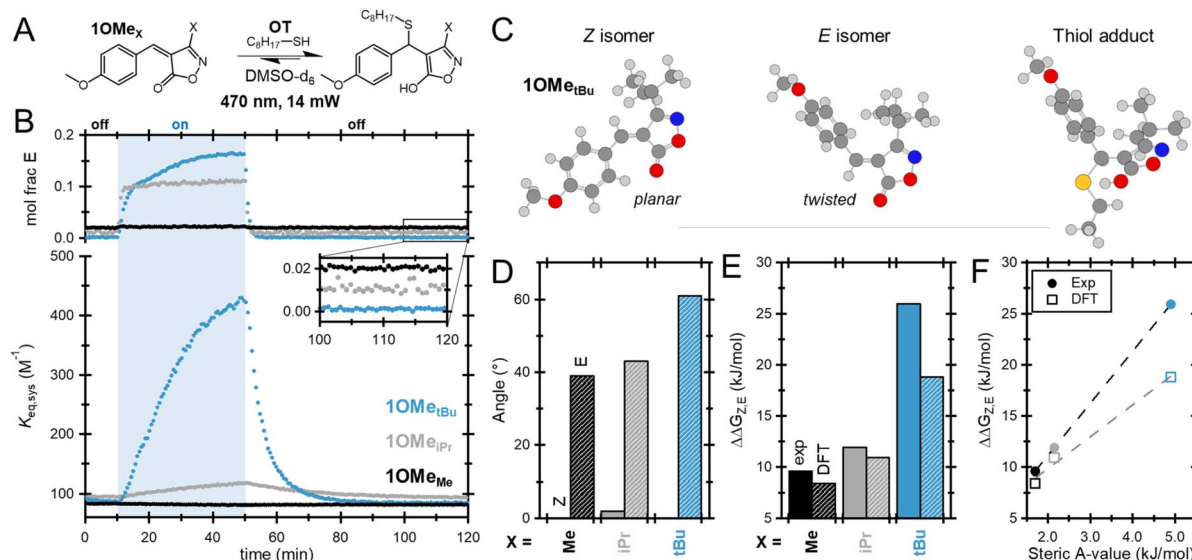
Fig. 6 (A) Equilibrium between **1OMe$_X$** acceptors and **OT**. (B) Mole fraction of the Z isomer and overall system K_{eq} ($K_{eq,sys}$) of **1OMe$_X$** equilibrated with **OT** during the NMR photoisomerization experiment. (C) Conformations of Z and E isomers as well as the thiol-adduct of **1OMe$_{tBu}$**. (D) Dihedral angles between the β-phenyl ring and α,β-unsaturated bond of Z (solid) and E (striped) isomers of **1OMe$_X$** acceptors. (E) $\Delta\Delta G$ Z and E isomers of **1OMe$_X$** acceptors and determined from experimental values (solid) and computations (striped). (F) $\Delta\Delta G$ of Z and E isomers of **1OMe$_X$** acceptors versus steric A-values of −X.
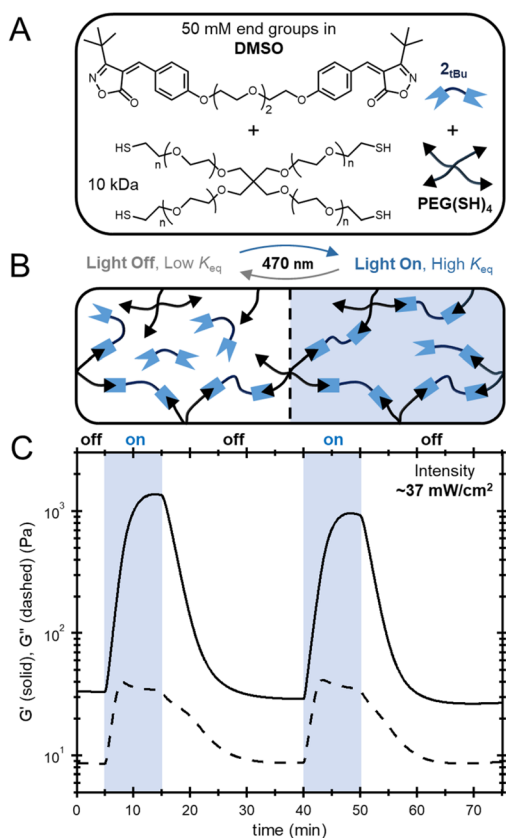

Fig. 7 (A) Chemical structures used in the synthesis of the organogel. (B) Diagram demonstrating increase in thiol-bonding and network connectivity upon irradiation. (C) Storage and loss moduli of the organogel during cycles of irradiation (470 nm) and darkness.

Having confirmed that the photoisomerization of these tM acceptors can be used to manipulate $K_{eq,sys}$, the next goal was to explore if this effect could also be observed in dynamic polymer networks. Upon exposure to light, the increase in $K_{eq,sys}$ would lead to increased crosslink density and modulus while dark periods would restore the initial properties, akin to recently reported light-stabilized dynamic materials.[50] To this end, a dynamic organogel was targeted. As the largest light-induced changes in K_{eq} were measured in the **1OMe$_{tBu}$** system, a ditopic species, **2$_{tBu}$**, was prepared by connecting through ether bonds, electronically similar to methoxy −R groups. With the ditopic monomer in hand, organogel samples were prepared by mixing **2$_{tBu}$** and a thiol-terminated 4-arm poly(ethylene glycol) (**PEG(SH)$_4$**, M_n = 10 kDa) macromonomer in DMSO (targeting 50 mM end group concentration). After mixing, the solution was equilibrated in the dark overnight, yielding a soft gel (Fig. 7A and B). The 50 mM end group concentration was chosen to yield a bonded fraction of ca. 0.61 (assuming a $K_{eq,Z}$ of 85 M^{-1}), close to the predicted critical gelation conversion by Flory–Stockmayer theory (ca. 0.58). After formation, the sample was loaded into a rheometer equipped with a 470 nm collimated LED and its mechanical properties were evaluated using small amplitude oscillatory shear rheology (setup shown in Fig. S12). Prior to irradiation, the sample exhibited a storage modulus of just over 30 Pa. Gratifyingly, exposure to 470 nm light was found to significantly increase the modulus of the sample, which plateaued at just over 1.2 kPa (Fig. 7C). Upon turning the light off, the sample was subjected to an additional on/off cycle, producing nearly identical results, with a ca. 40-fold increase in G' during light exposure and subsequent return to equilibrium after the light was turned off.

Conclusions

In summary, a new dynamic tM acceptor platform with photo-controllable K_{eq} has been developed using a molecular design in which both the photoswitchable and dynamic chemistry moieties are one and the same. Critically, these light sensitive DCC motifs can be readily prepared and derivatized through simple reactions, allowing tuning of the baseline K_{eq} and the overall photo-response. This isomerization-driven K_{eq} enhancement is tunable through steric bulk on the isoxazolone ring, with larger substituents producing more pronounced changes. In addition, it is shown that incorporation of this motif into organogels allows for impressive stiffening (ca. $40\times$ increase in the storage modulus) upon light irradiation. Critically, this direct photo-isomerization approach should be amenable to other dynamic bonding motifs, greatly expanding opportunities for applying light-responsive dynamic covalent chemistry.

Author contributions

Conceptualization: N. D. D., A. E. C, C. C., and S. J. R. Methodology: N. D. D., N. R. B., C. C., and S. J. R. Investigation: N. D. D., A. E. C., N. R. B., and C. C. Visualization: N. D. D. Writing – original draft: N. D. D., A. E. C., and S. J. R. Writing – review and editing: N. D. D., A. E. C., N. R. B., C. C., J. J. dP., S. A. S., and S. J. R. Funding acquisition: S. J. R., S. A. S., and J. J. dP.

Conflicts of interest

There are no conflicts to declare.

Data availability

The data that support the findings of this study are available from the corresponding authors upon reasonable request.

Additional data supporting this work can be found in the supplementary information (SI). Supplementary information: experimental procedures, UV-Vis spectra, NMR data, computational details, and rheology data. See DOI: **https://doi.org/10.1039/d5sc06704a**.

Acknowledgements

References

1 S. J. Rowan, S. J. Cantrill, G. R. L. Cousins, J. K. M. Sanders and J. F. Stoddart, *Angew. Chem., Int. Ed.*, 2002, **41**, 898–952.

2 S. Ulrich, *Acc. Chem. Res.*, 2019, **52**, 510–519.

3 T. Xue, Y. Li, M. Torre, R. Shao, Y. Han, S. Chen, D. Lee and D. S. Kohane, *Angew. Chem.*, 2024, **136**, e202406158.

4 S. Lamping, T. Otremba and B. J. Ravoo, *Angew. Chem., Int. Ed.*, 2018, **57**, 2474–2478.

5 E. Du, M. Li, B. Xu, Y. Zhang, Z. Li, X. Yu and X. Fan, *Macromolecules*, 2024, **57**, 672–681.

6 C. J. Kloxin and C. N. Bowman, *Chem. Soc. Rev.*, 2013, **42**, 7161–7173.

7 J. Demarteau, A. R. Epstein, P. R. Christensen, M. Abubekerov, H. Wang, S. J. Teat, T. J. Seguin, C. W. Chan, C. D. Scown, T. P. Russell, J. D. Keasling, K. A. Persson and B. A. Helms, *Sci. Adv.*, 2022, **8**, eabp8823.

8 E. Ghimire, C. A. Lindberg, T. D. Jorgenson, C. Chen, J. J. De Pablo, N. D. Dolinski and S. J. Rowan, *Macromolecules*, 2024, **57**, 682–690.

9 C. Shao, M. Wang, H. Chang, F. Xu and J. Yang, *ACS Sustain. Chem. Eng.*, 2017, **5**, 6167–6174.

10 S. Yang, X. Du, S. Deng, J. Qiu, Z. Du, X. Cheng and H. Wang, *Chem. Eng. J.*, 2020, **398**, 125654.

11 Q. Zhou, Z. Sang, K. K. Rajagopalan, Y. Sliozberg, F. Gardea and S. A. Sukhishvili, *Macromolecules*, 2021, **54**, 10510–10519.

12 S. Ji, W. Cao, Y. Yu and H. Xu, *Adv. Mater.*, 2015, **27**, 7740–7745.

13 M. J. Suazo and J. M. Torkelson, *ACS Appl. Polym. Mater.*, 2024, **6**, 9209–9218.

14 D. Montarnal, M. Capelot, F. Tournilhac and L. Leibler, *Science*, 2011, **334**, 965–968.

15 J. L. Self, N. D. Dolinski, M. S. Zayas, J. Read De Alaniz and C. M. Bates, *ACS Macro Lett.*, 2018, **7**, 817–821.

16 S. Wang and M. W. Urban, *Nat. Rev. Mater.*, 2020, **5**, 562–583.

17 A. G. Orrillo and R. L. E. Furlan, *Angew. Chem., Int. Ed.*, 2022, **61**, e202201168.

18 J. J. Lessard, K. A. Stewart and B. S. Sumerlin, *Macromolecules*, 2022, **55**, 10052–10061.

19 J. O. Holloway, C. Taplan and F. E. Du Prez, *Polym. Chem.*, 2022, **13**, 2008–2018.

20 V. Zhang, B. Kang, J. V. Accardo and J. A. Kalow, *J. Am. Chem. Soc.*, 2022, **144**, 22358–22377.

21 F. Van Lijsebetten, T. Debsharma, J. M. Winne and F. E. Du Prez, *Angew. Chem., Int. Ed.*, 2022, **61**, e202210405.

22 M. Kathan and S. Hecht, *Chem. Soc. Rev.*, 2017, **46**, 5536–5550.

23 J. V. Accardo and J. A. Kalow, *Chem. Sci.*, 2018, **9**, 5987–5993.

24 J. V. Accardo, E. R. McClure, M. A. Mosquera and J. A. Kalow, *J. Am. Chem. Soc.*, 2020, **142**, 19969–19979.

25 Y. You, Y. Yang, Y. Lv, H. Ye, H. Lu, Y. Zeng and L. You, *Chin. J. Chem.*, 2025, **43**, 1627–1634.

26 K. Kim, H. J. Cho, J. Lee, S. Ha, S. G. Song, S. Kim, W. S. Yun, S. K. Kim, J. Huh and C. Song, *Macromolecules*, 2018, **51**, 8278–8285.

27 D. N. Barsoum, V. C. Kirinda, B. Kang and J. A. Kalow, *J. Am. Chem. Soc.*, 2022, **144**, 10168–10173.

28 A. Drichel, Y. Garmshausen and S. Hecht, *Angew. Chem., Int. Ed.*, 2025, **64**, e202419531.

29 G. Jiang, Y. Hai, H. Ye and L. You, *Org. Chem. Front.*, 2022, **9**, 1343–1353.

30 K. Broi, F. Grabowski, S. Esser, J. Dörr, A. Pich and S. Hecht, *Angew. Chem., Int. Ed.*, 2025, e202510141.

31 A. B. Lowe, *Polym. Chem.*, 2010, **1**, 17–36.

32 B. Zhang, Z. A. Digby, J. A. Flum, P. Chakma, J. M. Saul, J. L. Sparks and D. Konkolewicz, *Macromolecules*, 2016, **49**, 6871–6878.

33 P. Chakma, L. H. Rodrigues Possarle, Z. A. Digby, B. Zhang, J. L. Sparks and D. Konkolewicz, *Polym. Chem.*, 2017, **8**, 6534–6543.

34 J. S. A. Ishibashi and J. A. Kalow, *ACS Macro Lett.*, 2018, **7**, 482–486.

35 K. M. Herbert, P. T. Getty, N. D. Dolinski, J. E. Hertzog, D. De Jong, J. H. Lettow, J. Romulus, J. W. Onorato, E. M. Foster and S. J. Rowan, *Chem. Sci.*, 2020, **11**, 5028–5036.

36 Y. Zhong, Y. Xu and E. V. Anslyn, *Eur. J. Org Chem.*, 2013, **2013**, 5017–5021.

37 A. E. Crolais, N. D. Dolinski, N. R. Boynton, J. M. Radhakrishnan, S. A. Snyder and S. J. Rowan, *J. Am. Chem. Soc.*, 2023, **145**, 14427–14434.

38 T. M. FitzSimons, F. Oentoro, T. V. Shanbhag, E. V. Anslyn and A. M. Rosales, *Macromolecules*, 2020, **53**, 3738–3746.

39 K. Thapa, T. M. FitzSimons, M. U. Otakpor, M. M. Siller, A. D. Crowell, J. E. Zepeda, E. Torres, L. N. Roe, J. Arts,

A. M. Rosales and T. Betancourt, *ACS Appl. Mater. Interfaces*, 2023, **15**, 52180–52196.

40 A. D. Crowell, T. M. FitzSimons, E. V. Anslyn, K. M. Schultz and A. M. Rosales, *Macromolecules*, 2023, **56**, 7795–7807.

41 G. L. Jackson, J. M. Dennis, N. D. Dolinski, M. Van Der Naald, H. Kim, C. Eom, S. J. Rowan and H. M. Jaeger, *Macromolecules*, 2022, **55**, 6453–6461.

42 H. Kim, M. Van Der Naald, N. D. Dolinski, S. J. Rowan and H. M. Jaeger, *Soft Matter*, 2023, **19**, 6797–6804.

43 H. Kim, M. Van Der Naald, F. A. Braaten, T. A. Witten, S. J. Rowan and H. M. Jaeger, *Soft Matter*, 2024, **20**, 6384–6389.

44 N. R. Boynton, J. M. Dennis, N. D. Dolinski, C. A. Lindberg, A. P. Kotula, G. L. Grocke, S. L. Vivod, J. L. Lenhart, S. N. Patel and S. J. Rowan, *Science*, 2024, **383**, 545–551.

45 N. D. Dolinski, R. Tao, N. R. Boynton, A. P. Kotula, C. A. Lindberg, K. J. Petersen, A. M. Forster and S. J. Rowan, *ACS Macro Lett.*, 2024, 174–180.

46 A. E. Crolais, C. Chen, J. Gao, N. D. Dolinski, Y. Xu, J. J. De Pablo, S. A. Snyder and S. J. Rowan, *J. Org. Chem.*, 2025, **90**, 4037–4045.

47 N. D. Dolinski, Z. A. Page, F. Eisenreich, J. Niu, S. Hecht, J. Read de Alaniz and C. J. Hawker, *ChemPhotoChem*, 2017, **1**, 125–131.

48 Y. Zhao and D. G. Truhlar, *Theor. Chem. Acc.*, 2008, **120**, 215–241.

49 M. Cossi, N. Rega, G. Scalmani and V. Barone, *J. Comput. Chem.*, 2003, **24**, 669–681.

50 H. A. Houck, E. Blasco, F. E. Du Prez and C. Barner-Kowollik, *J. Am. Chem. Soc.*, 2019, **141**, 12329–12337.